IJASS
International Journal of
Aeronautical and Space Sciences

ORIGINAL PAPER

CrossMark

A Development and Assessment of Variable-Incidence Angle Vortex Generator at Low Reynolds Number of ~ 5×10⁴

Ho-Hyun Kim[1] · Ho-Young Kim[1] · Jong-Seob Han[1] · Jae-Hung Han[1]

Abstract

The aerodynamic benefit for conventional vortex generator (VG) is often counterbalanced by the appearance of parasite drag. An immovable installation similar to a fixture also limited its application. To overcome those issues, this paper proposes a variable-incidence-angle vortex generator (VIVG). Counter-rotated miniature gears with a single rack-pinion system adjust the incidence angle of the VIVG, thereby precisely control mixing flux at boundary layer interface with minimizing the parasite drag. The variable incidence angle of the VIVG was then examined to evaluate the applicability of the VIVG at low Reynolds number. The VIVG was mounted on a NACA 0015 airfoil, and a low-turbulence blowing type wind tunnel was employed. We found that the VIVG effectively eliminated laminar separation bubbles, and suppressed separation at Reynolds number of 5.4×10^4; excessive lift production at low Reynolds number became similar to a theoretical value of potential flow ($C_L = 2\pi\alpha$). It was also found that the VIVG can reduce the drag in the pre-stall region at the low Re with small incidence angles, providing a noticeable increment of the lift-to-drag ratio. The large incidence angle of VIVG was also useful both to extend the stall point and to produce higher lift force with reasonable efficiency. These clearly indicate that the VIVG is applicable for performance improvement of aerodynamic devices operated in low Reynolds number flow fields.

Keywords Flow control · Vane-type vortex generator · Variable-incidence-angle vortex generator · Low Reynolds number flow · Laminar flow separation

1 Introduction

Various aerodynamic devices in low Reynolds number flow fields, such as small-scale wind turbines [1], always suffer a certain drawback due to a scale effect [2–4]. This drawback commonly stems from a laminar-dominant flow field with a lack of inertia, which is insufficient to overcome the adverse pressure gradient over the maximum thickness of the aerodynamic devices. In an airfoil, for instance, stall appears at much lower angles of attack, and lift is substantially reduced in the pre-stall region [5]. Intricate events in the boundary layer, such as laminar separation, transition in free shear layer, reattachment, laminar separation bubbles (LSB), and leading-edge bubbles (LEB) are other features accelerating the reduction of the aerodynamic performance [6, 7].

Among these, LSB is known as the primary source degrading the overall aerodynamic performance; LSB commonly results in undesired fluctuation and discontinuity in the aerodynamic lift, accompanied with substantial drag [4]. Highly sensitive characteristics of the LSB depending on both the angle of attack and the Reynolds number also create an oscillating force with back-and-forth movement of the LSB in the pre-stall region, eventually destabilizing the negative pressure distribution on the suction side of aerodynamic devices with dynamic transition and separation points [8–10].

Several active flow control devices such as excitation actuators [11–13], suction and blowing actuators [14–16], and synthetic jet actuators [17, 18] have been investigated to suppress the flow separation and thereby improve the aerodynamic performances. Micro driving instruments such as piezoceramic actuators [19] were inserted in active flow control devices to produce massive flux, which induces strong mixing at the boundary layer interfaces, thereby supplying additional energy to the boundary layer in a straightforward way. Therefore, these give us reliable improvement of aerodynamic performance with arbitrary control of the volume

✉ Jae-Hung Han
jaehunghan@kaist.ac.kr

[1] Department of Aerospace Engineering, KAIST, Daejeon, Republic of Korea

of fluid, mixing strength, and excitation level for each circumstance. However, delicate mechanical parts requiring additional energy resources to operate, which degrade the overall efficiency, remain the biggest weakness for the application of such devices.

Use of vortex generators (VGs) could be an alternate way to control boundary layer separation. These devices are usually only constructed in simple shapes such as zig-zag trips, wedges, wishbones, and wheelers [20–23], and have been widely used to control the flow separation in various aerodynamic devices such as thick airfoil sections near the hubs of large wind turbines [22]. These devices also guarantee adequate flow control capability to prevent the flow separation [24, 25]. The use of VGs, however, requires an in-depth consideration of device shape and dimensions, because it permanently accompanies with a parasite drag, which degrades overall aerodynamic performance. Griffin [26], for example, tested the several VG configurations on a two-dimensional section of a wind turbine blade and showed that the VGs could increase an annual energy production up to 10%, but always gives rise to a substantial dynamic load. The recent study on the effect of VGs [27] further showed that the VGs could offset the performance degradation due to a surface contamination, but did not bring out better aerodynamic performance than the clean case.

The previous results showing an insufficient performance of the VGs may stem from non-optimized adoption in the initial design stage. The shapes and dimensions are more significant in low Reynolds number flow fields, in which intricate flow structures become dominant [3]. In particular, the incidence angle between two vanes of VGs, which is the preliminary parameter determining the strength of the counter-rotating vortex pair, should be investigated in advance to achieve higher efficiency without losing the overall aerodynamic performance of aerodynamic devices in low Reynolds number flow fields.

In this paper, we propose a variable-incidence-angle vortex generator (VIVG). This consists of counter-rotated miniature gears with a single rack-pinion system, which can be installed under aerodynamic devices, adjust the arbitrary incidence angle of vanes with minimizing the parasite drag for each circumstance. We then evaluated the effect of the incidence angle of VIVG on the aerodynamic characteristics of a NACA 0015 airfoil at Reynolds number of 5.4×10^4. For a wide range of incidence angles and angles of attack, a low turbulence blowing type wind tunnel and a balance system were employed to measure the lift and drag of the airfoil with the VIVG. It was found that the VIVG is effective at suppressing the laminar separation and eliminating the LSB. It was also found that the VIVG can provide better efficiency in most pre-stall regions with a small incidence angle. Large incidence angle was also useful, both to extend the stall point and to produce maximum lift with reasonable

efficiency. These all imply that the VIVG can provide better aerodynamic performance at low Reynolds number.

2 Experimental Setup and Procedure

Lin [24] and Ashill et al. [25] collected literature dealing with the flow control performance of various shapes of VGs and other flow control devices; they reported that a vane-type VG had the most excellent flow control performance. This vane-type VG is composed of a pair of bisymmetrical fins, like mirror images of each other, with a certain incidence angle to induce a counter-rotating vortex pair.

Figure 1 shows the shape and dimensions of the VIVG installed on a NACA 0015 airfoil. The airfoil had a chord length c of 150 mm and a span of 294 mm. This airfoil was fabricated by a 3d printer with poly lactic acid filament. In order to smooth out the surface of the airfoil, polyester putty and sand paper with grit levels from P100 to P2000 were used.

The VIVG in this paper was composed of fifteen pairs of vanes and was installed at $0.2c$ from the leading edge. Each vane of the VIVG had a triangular shape with height h and length $l = 2h$, where $h = 0.02c$. The distance between fins, s, and the spatial interval of the pair of vanes, z, are $2.5h$ and $6.0h$, respectively. These vanes were mounted on the shaft of each counter-rotating miniature gear. Here, two bearings supporting each shaft prevented the misalignment of the fins. Each pair of vanes had one additional pinion gear, which meshed with a rack gear; using the single linear input on the rack gear, the incidence angles of the entire set of vanes were automatically adjusted.

Figure 2 shows the test setup in this study. A blowing type wind-tunnel at KAIST, which had a test section of 1000 mm (L) × 300 mm (W) × 300 mm (H) was employed. The maximum speed of the freestream is 30 m/s, with a turbulence intensity less than 0.8%.

To accurately adjust the angle of attack, the airfoil was mounted on a stepper motor, which had a resolution of 0.005° (A200K-M599-G7.2, Autonics Co.). Two single-axis bending beam type loadcells were installed between the airfoil and the stepper motor to measure the lift and drag. Each loadcell (OBU-1, Bongshin) had a measurement range of ± 1 kgf and resolution of 0.02% at maximum load, and were connected to signal amplifiers (DN AM310, Dacell) and to a DAQ system (PXIe-6361, NI) for data acquisition. To avoid unpredictable effects from misalignment and/or backlashes in the apparatus, as shown in Fig. 2, a calibration matrix for the loadcells was determined under mounted condition; these showed identical values to those given by the manufacturer.

The freestream speed was fixed at 5.0 m/s, corresponding to a Reynolds number of 5.4×10^4. The aerodynamic forces were measured in a range of angle of attack of − 10 to 20° at
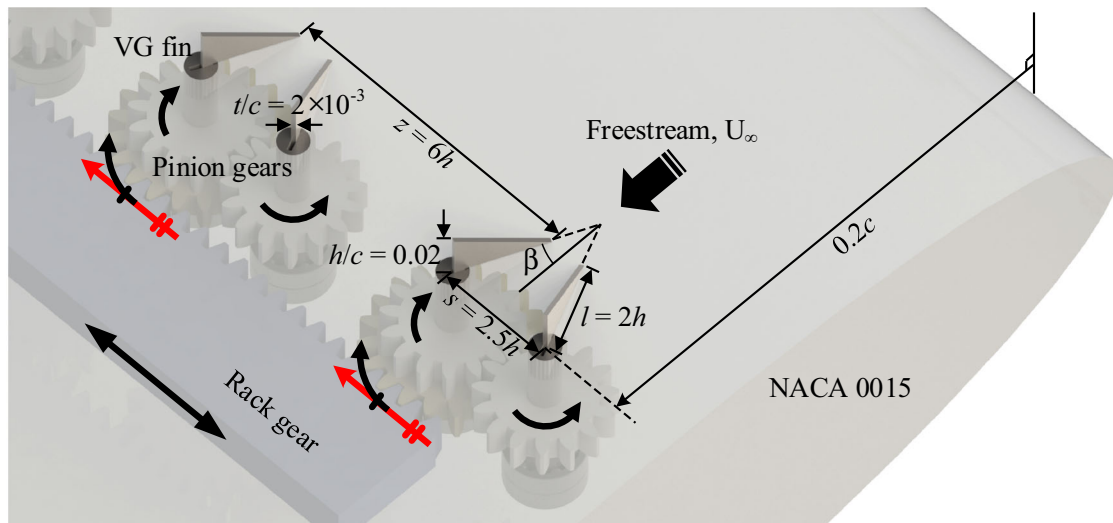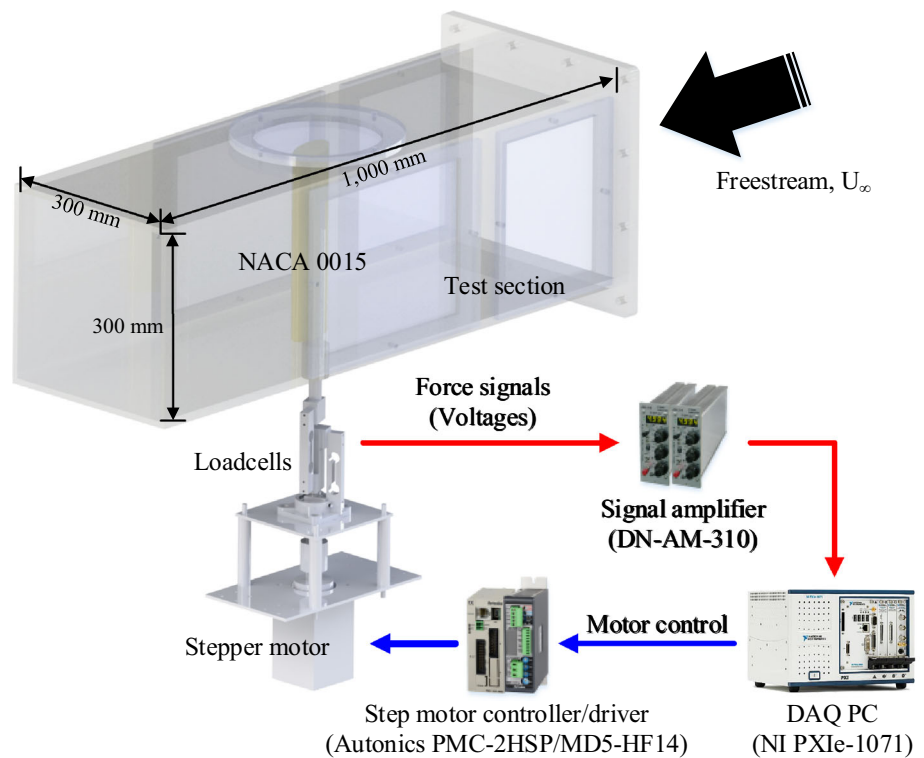
Fig. 1 Schematic of the VIVG installed on NACA 0015 airfoil

**Fig. 2** Experimental setup

intervals of 0.5° (a total of 61 angles of attack); the incidence angles of the VIVG started from 0 to 38.2° at intervals of 7.65° (a total of 6 incidence angles); these were controlled by a high-precision servo motor (XH-430-W210R, Robotis®) mounted in the airfoil. The data in each case was collected for 30 s with a sampling frequency of 1 kHz. An in-house code written in LabVIEW™ was used to control the stepper motor and measurement process; this automatically shifted the angle of attack to the next sequence with fixed spatial and temporal intervals (0.5° and 30 s) for each designated

incidence angle. 5000 data samples were extracted from the data for white noise reduction, and were calibrated to extract the aerodynamic forces. Each force was decomposed to lift and drag with respect to angles of attack, and normalized to the aerodynamic coefficients using Eqs. (1) and (2),

$$C_L = \frac{2L}{\rho U_\infty^2 S} = \frac{2(F_X \sin\alpha + F_Y \cos\alpha)}{\rho U_\infty^2 S}, \tag{1}$$

$$C_D = \frac{2D}{\rho U_\infty^2 S} = \frac{2(F_X \cos\alpha - F_Y \sin\alpha)}{\rho U_\infty^2 S}. \tag{2}$$

Fig. 3 Ensemble averages and standard deviation SD for the clean airfoil

(a) Ensemble averages

(b) SD in the C_L
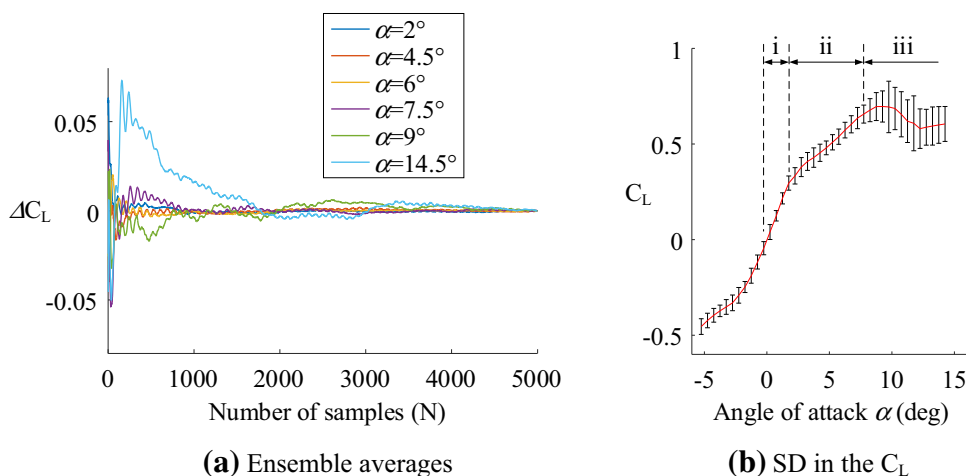
Type-A measurement uncertainty was evaluated [28]. The resolution of the stepper motor of $\pm 0.005°$ resulted in a value of $\pm 0.0167\%$ of angle of attack. A change in temperature from 6.55 to 7.75 °C also gave us the density of 1.260 ± 0.005 kg/m^3 (0.397%). The freestream velocity had a range of 5.0 ± 0.05 m/s ($\pm 1.00\%$). Including the resolution of the loadcells given by the manufacturer (± 0.002 N; 0.375%), overall uncertainty level of each coefficient became $\pm 2.18\%$ of the maximum lift.

Figure 3a and b show ensemble averages of the lift coefficient C_L for the selected angles of attack α and their standard deviations SD for the airfoil without the VIVG (clean airfoil). Here, ΔC_L denotes the ensemble-averaged C_L subtracted from the mean values in each α, as shown in Eq. (3),

$$\Delta C_L = C_L - \frac{\sum_{i=1}^{N} C_{L,i}}{N}. \tag{3}$$

At $\alpha < 6°$, the ΔC_L did not need a large number of samples to converge. The ΔC_L at $\alpha > 6°$ required relatively more samples due to both the separation and the turbulent wake, but 5000 samples still seemed to be sufficient to converge. This implies that white noise during measurements was properly isolated from the results, and SD can inform us of the perturbation and/or the turbulent characteristics, as shown in Fig. 3b. We found that the overall aerodynamic characteristics could be briefly classified into three regions with respect to the level of SD; (i) fully laminar flow with small α ($0 < \alpha < 2.0$), (ii) intermediate region that contains relatively large-scale LSB and/or LEB ($2.0 < \alpha < 7.5$), and iii) fully separated flow with strong fluctuation ($\alpha > 7.5$). These results are clearly in line with the previous study that demonstrated five distinctive flow structures for similar Reynolds number flow fields [6].

To validate both our results and the measurement system, we further compared the C_L to that of the previous study [6].

Figure 4a shows two C_L curves obtained by two different wind-tunnel facilities. Here, the VIVG were disassembled from the surface for a fair comparison (clean case). In the pre-stall region ($0 < \alpha < 7.5°$), the two curves show excellent agreement. Both curves exhibit two features in common; excessive lift production beyond that predicted by the potential flow theory ($C_L = 2\pi\alpha$) at $0 < \alpha < 3.5°$, and a degraded growth rate at $3.5 < \alpha < 7.5°$. These are typical flow characteristics at low Reynolds number [6, 9, 10]; the existence of LSB and a barely separated boundary layer over the LSB produced the excessive lift at lower α, and early-starting separation before the stall angle degraded the growth rate in the C_L (refer to Figs. 4bii, iii for the flow structures in detail). In the post-stall region ($\alpha > 7.5°$), however, the two curves showed comparable disagreement. The C_L in this study had a relatively gentle arc at the stall, and maintained a C_L level after the stall higher than that of the previous study [6]. Huang and Lee [6] reported that a strong turbulent intensity in the freestream resulted in the higher C_L values after the stall, and C_L dramatically increased when the turbulent intensity reached 0.4%. Therefore, it can be concluded that the higher turbulent intensity of $\sim 0.8\%$ in this study was the main source maintaining the strong aerodynamic lift in the post-stall region. Such intricate aerodynamic characteristics was also an appropriate test bed to evaluate the VIVG developed in this study.

3 Results and Discussion

Figure 5 displays the $C_L - \alpha$ curves for the selected incidence angles β. It was found that regardless of the level of β, the lift increment in the clean airfoil was nearly eliminated by the VIVG. All curves with VIVG, therefore, obeyed the theoretical level of C_L (dashed line), at least in the range of $0 < \alpha < 3.5°$. The other increment due to LEB at $3.5 < \alpha < 7.5°$ also vanished (refer to Fig. 4biii). Overall tendencies of C_L

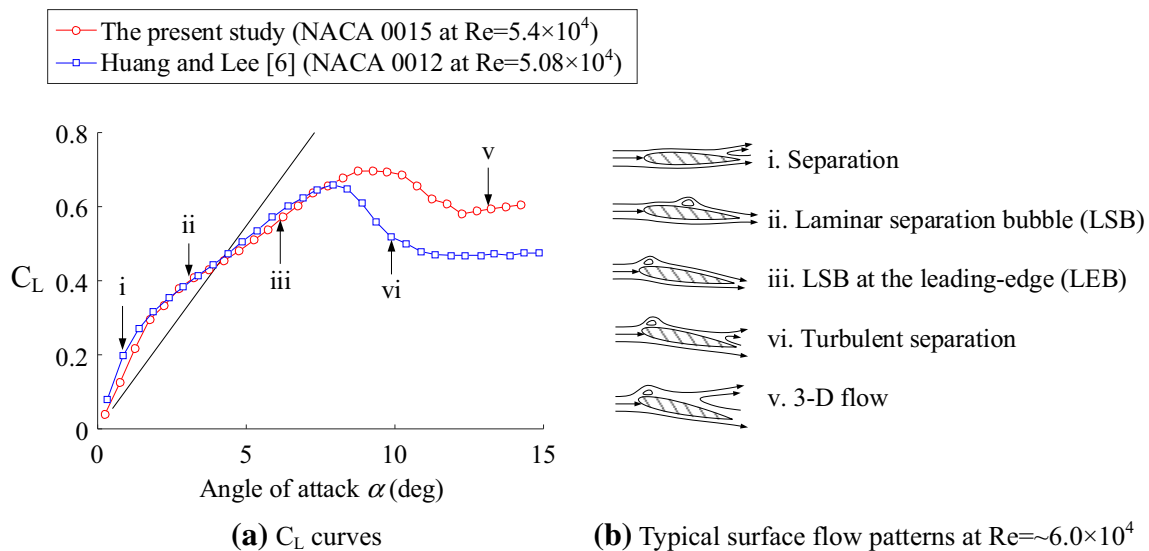**(a)** C_L curves   **(b)** Typical surface flow patterns at Re=~6.0×10^4

Fig. 4 Comparison of C_L with the previous study [6]; Fig. 4b was reproduced by the authors

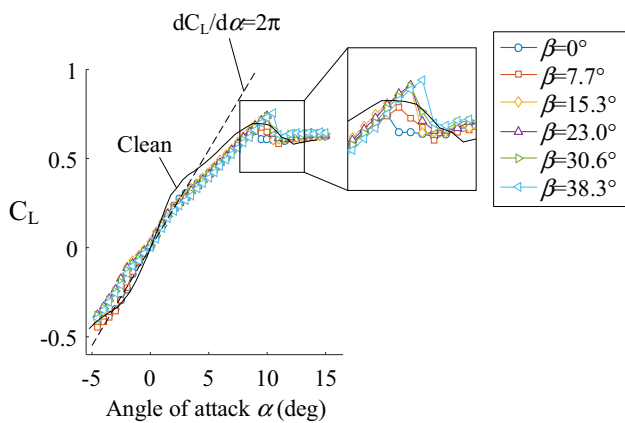**Fig. 5** C_L depending on β

Fig. 6 C_D depending on β

with VIVG, therefore, showed monotonic increments in the pre-stall region. Note that the LSB was deeply dependent on the turbulent intensity [6]. This implies that using the VIVG can give us robust lift production for various levels of atmospheric turbulence. The linear growth of C_L in the pre-stall region also implies easier prediction via an aerodynamic model.

Figure 5 also shows that using sharp β postponed the stall, thereby producing higher lift at higher α. In the case of $\beta = 38.3°$, for example, C_L had a 14.3% higher value (C_L ~0.75 at $\alpha = 10°$) than that of the VIVG with $\beta = 0°$ (C_L ~0.66 $\alpha = 8.5°$); C_L had an 8.3% higher value than that of the clean airfoil case (C_L ~0.70 $\alpha = 9°$). This clearly indicates that the VIVG was also useful to suppress turbulent separation in low Reynolds number flow fields (refer to Fig. 4bv for the flow structure in detail).
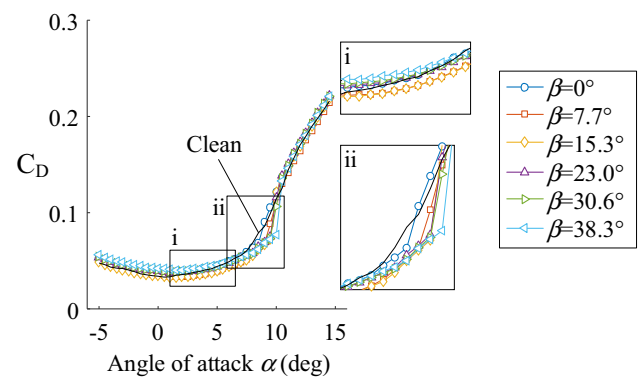
The same influences of the VIVG were found in the drag coefficients C_D. Figure 6 shows C_D with respect to β. One noteworthy feature was the drag reductions at $0 < \alpha < 8.0°$, with small β values of 7.7 and 15.3° (Fig. 4i). The VIVG in this range of α attenuated C_D to~11.3%. This informs us that the presence of LSB at low Reynolds number could induce considerable drag, which is much stronger than that of the parasite drag of each vane of the VIVG. This also clearly indicates that eliminating LSB with adequate β, which can be achieved by the VIVG, can significantly reduce aerodynamic drag in the pre-stall region.

The VIVG also extended the pre-stall region, similar to the case of C_L. As shown in Fig. 6ii, from $\alpha = 8.5°$, the stall point was extended to $\alpha = 10°$ with $\beta = 38.3°$. This shows that the VIVG with an appropriate β can enhance the range of operation of aerodynamic devices at low Reynolds number.

Figure 7 shows the lift-to-drag ratio L/D. We found that the VIVG is able to maintain the overall efficiency with small β at $0 < \alpha < 2.5°$, it even eliminated LSB and reduced the lift
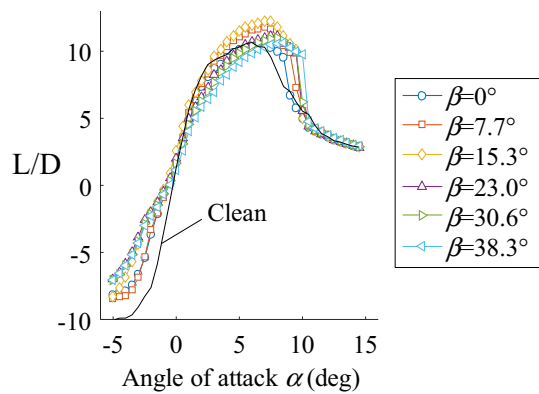
Fig. 7 Lift-to-drag ratios depending on β

augmentation (refer to Fig. 4bii for the LSB). This informs us that LSB is always accompanied by heavy drag even it can augment the lift, and using the VIVG with adequate β to eliminate LSB can be a good option to preserve the efficiency. It was also found that small β values of 7.7 and 15.3° elevated L/D in most ranges of α, from 2.5° to the stall angle. At $\alpha = 6°$, for example, L/D with $\beta = 15.3$ reached 11.96, which is a 12.2% higher efficiency than that of the clean case ($L/D = 10.66$). This clearly indicates that adopting the VIVG is highly recommended for aerodynamic devices operating at low Reynolds number. In particular, the VIVG would be very suitable for energy harvesting systems such as wind turbines [1, 22].

Using the VIVG with high β also guaranteed better efficiency near the stall angle. The L/D of 9.75 with $\beta = 38.3°$ at the stall angle was almost twice the value of the clean airfoil case. Although this L/D was only 79.5% of the maximum value of L/D (at $\beta = 15.3°$ and $\alpha = 7.5°$), it is still useful when heavy aerodynamic lift is necessary.

Excessive mixing flux of the vortex pair generated by the active flow control devices frequently reduces the overall aerodynamic performance due to the growth of parasite drag [26, 27, 29, 30]. The L/D in this study indicates that the variable incidence angles are sufficient to obtain better aerodynamic performance without losing efficiency for the various circumstance. In addition, the VIVG developed in this study would be great tools to control low Reynolds number flow fields.

4 Conclusion

In this paper, we propose the VIVG, which provide adjustable incidence angle of vanes thereby minimizing the parasite drag, which permanently appears in the conventional VGs. We then examined incidence angles of the VIVG and its flow control performance in low Reynolds number flow fields of 5.4×10^4. The NACA 0015 airfoil was employed, and the

clean airfoil was also examined for comparison. The results from the clean airfoil clearly show intricate aerodynamic characteristics such as excessive C_L and lower growth rate in the pre-stall region due to laminar separation and ensuing LSB/LEB. These results were in an excellent agreement with the previous study, which showed intricate boundary-layer-events depending on the angle of attack. We found that using the VIVG with adequate incidence angles is highly recommended for performance improvement of aerodynamic devices, which operate in low Reynolds number flow fields. The VIVG was capable of stabilizing C_L in the pre-stall region, so that it became similar to a theoretical value of potential flow. The VIVG also effectively eliminated LSB and suppressed separation. The VIVG with small β significantly reduced the drag in most pre-stall regions; this resulted in a substantial improvement of L/D. The VIVG with large β was also useful to extend the stall point, thereby achieving both maximum lift and moderate efficiency.

References

1. McTavish S, Feszty D, Nitzsche F (2013) Evaluating reynolds number effects in small-scale wind turbine experiments. J Wind Eng Ind Aerodyn 120:81–90. https://doi.org/10.1016/j.jweia.2013.07.006
2. Tani I (1964) Low-speed flows involving bubble separations. Prog Aerosp Sci 5:70–103. https://doi.org/10.1016/0376-0421(64)90004-1
3. Lessaman PBS (1983) Low-reynolds-number airfoils. Annu Rev Fluid Mech 15:223–239. https://doi.org/10.1146/annurev.fl.15.010183.001255
4. Genç MS, Karasu İ, Açıkel HH, Akpolat MT (2012) Low Reynolds number flows and transition. In: Genç MS (ed) Low Reynolds number aerodynamics and transition. InTech, Rijeka, pp 1–28. https://doi.org/10.5772/31131
5. Alam MM, Zhou Y, Yang HX, Guo H, Mi J (2010) The ultra-low Reynolds number airfoil wake. Exp Fluids 48:81–103. https://doi.org/10.1007/s00348-009-0713-7
6. Huang RF, Lee HW (1999) Effects of freestream turbulence on wing-surface flow and aerodynamic performance. J Aircraft 36(6):965–972. https://doi.org/10.2514/2.2537
7. Rinoie K, Takemura N (2004) Oscillating behavior of laminar separation bubble formed on an aerofoil near stall. Aeronaut J 108(1081):153–163. https://doi.org/10.1017/S0001924000000063
8. Yang Z, Haan FL, Hui H (2007) An experimental investigation on the flow separation on a low-Reynolds-number airfoil,. AIAA-2007-0275, 45th AIAA Aerospace Sciences Meeting and Exhibit, Reno, NV, USA. https://doi.org/10.2514/6.2007-275
9. Kim D-H, Chang J-W, Chung J (2011) Low-Reynolds-number effect on aerodynamic characteristics of a NACA 0012 airfoil. J Aircraft 48(4):1212–1215. https://doi.org/10.2514/1.C031223

10. Genç MS, Karasu İ, Açıkel HH (2012) An experimental study on aerodynamics of NACA2415 aerofoil at low Re numbers. Exp Thermal Fluid Sci 39:252–264. https://doi.org/10.1016/j.exptherm flusci.2012.01.029

11. Yarusevych S, Kawall JG, Sullivan PE (2003) Effect of acoustic excitation on airfoil performance at low Reynolds numbers. AIAA J 41(8):1599–1601. https://doi.org/10.2514/2.2113

12. Yarusevych S, Sullivan PE, Kawall JG (2007) Effect of acoustic excitation amplitude on airfoil boundary layer and wake development. AIAA J 45(4):760–771. https://doi.org/10.2514/1.25439

13. Ricci R, Montelpare S, Silvi E (2007) Study of acoustic disturbances effect on laminar separation bubble by IR thermography. Exp Thermal Fluid Sci 31(4):349–359. https://doi.org/10.1016/j.e xpthermflusci.2005.08.007

14. Genç MS, Lock G, Kaynak Ü (2008) An experimental and computational study of low Re number transitional flows over an aerofoil with leading edge slat. In: AIAA-2008-8877, 26th Congress of International Council of the Aeronautical Sciences, Anchorage, Alaska, USA. https://doi.org/10.2514/6.2008-8877

15. Genç MS, Kaynak Ü, Yapici H (2011) Performance of transition model for predicting low Re aerofoil flows without/with single and simultaneous blowing and suction. Eur J Mech B Fluids 30(2):218–235. https://doi.org/10.1016/j.euromechflu.2010.11.00 1

16. Wahidi R, Bridges DH (2012) Effects of distributed suction on an airfoil at low Reynolds number. AIAA J 50(3):523–539. https://d oi.org/10.2514/1.J050913

17. Goodfellow SD, Yarusevych S, Sullivan P (2010) Low Reynolds number flow control over an airfoil using synthetic jet actuators. In: IMECE2010-39728, ASME 2010 international mechanical engineering congress and exposition, vancouver, British Columbia, Canada. https://doi.org/10.1115/imece2010-39728

18. Feero MA, Goodfellow SD, Lavoie P, Sullivan PE (2015) Flow reattachment using synthetic ject actuation on a low-Reynolds-number airfoil. AIAA J 53(7):2005–2014. https://doi.org/10.2514/1.J0536 05

19. Choi J, Jeon WP, Choi HC (2002) Control of flow around an airfoil using Piezoceramic actuators. AIAA J 40(5):1008–1010. https://d oi.org/10.2514/2.1741

20. Selig MS, Guglielmo JJ, Broeren AP, Giguere P (1996) Experiments on airfoils at low Reynolds numbers, AIAA-96-0062, 34th AIAA aerospace sciences meeting and exhibit, Reno, NV, USA. https://doi.org/10.2514/6.1996-62

21. Nickerson JD (1986) A study of vortex generators at low Reynolds numbers, AIAA-86-0155, 24th AIAA Aerospace Sciences Meeting, Reno, NV, USA. https://doi.org/10.2514/6.1986-155

22. Kerho M, Hutcherson S, Blackwelder RF, Liebeck RH (1993) Vortex generators used to control laminar separation bubbles. J Aircraft 3:315–319. https://doi.org/10.2514/3.46336

23. Seshagiri A, Cooper E, Traub LW (2009) Effects of vortex generators on an airfoil at low Reynolds numbers. J Aircraft 46(1):116–122. https://doi.org/10.2514/1.36241

24. Lin JC (1992) Control of low-speed turbulent separated flow over a backward-facing ramp. Ph.D. Dissertation, Old Dominion University, Norfolk, VA, USA

25. Ashill PR, Fulker JL, Hackett KC (2001) Research at DERA on sub boundary layer vortex generators (SBVGs). In: AIAA-2001-0887, 39th AIAA aerospace sciences meeting and exhibit, Reno, NV, USA. https://doi.org/10.2514/6.2001-887

26. Griffin DA (1996) Investigation of vortex generators for augmentation of wind turbine power performance. Technical Report NREL/SR-440-21399, NREL

27. Baldacchino D, Ferreira C, Tavernier DD, Timmer WA, van Bussel GJW (2018) Experimental parameter study for passive vortex generators on a 30% thick airfoil. Wind Energy 21:745–765. https://d oi.org/10.1002/we.2191

28. AGARD Working Group (1999) Standard: assessment of experimental uncertainty with application to wind tunnel testing. AIAA Standards/AIAA S-071A-1999, AIAA. https://doi.org/10.2514/4. 473647

29. Lin JC (1999) Control of turbulent boundary-layer separation using micro-vortex generators, AIAA-99-3404. In: 30th AIAA Fluid Dynamics Conference, Norfolk, VA, USA. https://doi.org/10.25 14/6.1999-3404

30. Lin JC (2002) Review of research on low-profile vortex generators to control boundary-layer separation. Prog Aerosp Sci 38(4–5):389–420. https://doi.org/10.1016/s0376-0421(02)00010-6